Watanabe and Iizuka *ROBOMECH Journal* (2023) 10:27
https://doi.org/10.1186/s40648-023-00265-9

ROBOMECH Journal

RESEARCH ARTICLE

Open Access

Experimental investigation of relationship between bearing capacity and vibration parameters for planetary exploration legged rovers

Tomohiro Watanabe[1*†] and Kojiro Iizuka[2†]

Abstract

In recent years, robots with leg mechanisms have received considerable attention as high-running planetary exploration rovers. Rovers undertaking planetary exploration require outstanding running performance to travel on loose ground on which they mostly slip and hardly move forward. The movement of the rover easily deforms the surface of loose ground. This problem can be solved by increasing the bearing capacity. The bearing capacity, the resistance force exerted on the rover legs when they make contact with the ground, needs to be sufficiently large to prevent legged rovers from slipping on loose ground. The bearing capacity can be increased by compaction of the ground by imparting vibrations. This study investigates the relationship between the bearing capacity in the horizontal direction and vibration parameters because this relationship offers valuable information for improving the running performance of legged rovers. First, we investigated the effect of changing the vibration parameters on the bearing capacity. Our experimental results show that the bearing capacity is related to vibration acceleration. These results suggest that the bearing capacity can be estimated from the vibration acceleration. Next, the frequency and amplitude were compared as vibration parameters to devise an efficient method for increasing the bearing capacity. The results of these experiments showed that high-amplitude vibrations increase the bearing capacity to a greater extent than high-frequency vibrations. The reason is that high-amplitude vibrations generate larger additional vibrations by the collision between the rod and the ground than high-frequency vibrations. This knowledge is valuable for selecting a suitable vibration that can efficiently increase the bearing capacity. This study suggests a method of facilitating further planetary exploration using legged rovers.

Keywords Planetary exploration, Legged rover, Vibration, Bearing capacity, Loose ground

Introduction

Planetary exploration is essential for human development. These explorations can help us probe the origins of planets and their sources of life. Exploiting the natural resources of other planets and extraterrestrial bodies is expected to solve natural resource issues on Earth. In this regard, many missions are expected to be undertaken to explore the moon. The Artemis program is underway to develop a base for the Moon [1] and plans to return astronauts to the lunar surface. In addition, the Smart Lander for Investigating Moon (SLIM) was launched on

†T. Watanabe, K. Iizuka: Equal contributors.

*Correspondence:
Tomohiro Watanabe
watanabe@eng.niigata-u.ac.jp
[1] Mechanical Engineering Program, Faculty of Engineering, Niigata University, 8050, Ikarashi 2no-cho, Nishi-ku, 950–2181 Niigata, Japan
[2] Department of Systems and Engineering and Science, Shibaura Institute of Technology, 307, Fukasaku, Minuma-ku, 337–8570 Saitama, Japan

September 2023, and the gateway, a platform orbiting the Moon, is currently under development [2, 3]. Therefore, the demand for exploration robots that can operate on lunar surfaces could be expected to increase. For example, the gateway plans to land robots on the surface of the Moon and the SLIM plans to carry the robots internally and deliver them to the surface of the Moon.

Exploration robots, known as rovers, are designed to move on the surfaces of planets or other extraterrestrial bodies. These robots have been used to successfully explore planets and have collected significant information. For example, the Mars Exploration Rover has identified traces of water on Mars [4]. This evidence points to the increasing possibility that life existed on Mars. Pathfinder, which landed on the surface of Mars, gathered meteorological information including the temperature, pressure, and wind on the planet [5]. Moreover, this rover analyzed the chemical compositions of the rocks and soil on Mars. Lunokhod 2, a rover developed by the Soviet Union, captured many photographs and television images of the Moon [6]. Many of the rovers were wheeled. However, the running performance of the current rovers must be improved to expand the area that can be explored. Viking, a probe that landed on Mars, surveyed the surface of this planet [7], which is characterized by many rocks with sizes of at least 30 cm. The area that conventional wheel-type rovers can explore is limited because it is difficult for them to traverse rough terrain on which they should avoid spending unnecessary time and being unable to move. Therefore, rovers must be able to move efficiently on rough terrain comprising inclines and rocks to ensure they are not restricted to a limited exploration area. Recently, robots with leg mechanisms have been investigated as exploration rovers with outstanding running performance. The Jet Propulsion Laboratory developed ATHLETE, which is a hexapod robot [8]. ATHLETE has good running performance on rough terrain because each leg has sufficient degrees of freedom for selecting the touch point with the ground. Moreover, legged robots are less affected by sinking into the loose soil on the ground than wheel-type robots because the leg mechanisms can separate them from the ground when moving. However, legged robots generally require more energy than wheel-type robots do. As a solution to this problem, the combination of a rover for long-distance travel with a legged robot to explore excessively rough terrain has been proposed [9, 10]. This mission style offers an efficient approach to increase the reachable exploration area. Thus, the demand for legged rovers can be expected to increase in future planetary exploration.

The surfaces of Mars and the Moon are not only rough but also loose. The ground on the surface is covered with loose soil, which is referred to as regolith. Moreover, the loose ground is uneven with many slopes because of the existence of craters and is easily deformed by an external force. Owing to the inherent characteristics of loose ground, legged rovers mostly slip because the motion of their legs deforms the surface of loose ground. Our previous study confirmed that the shear strength of the ground and sinkage of the rover legs increased when the loose ground was subjected to vibration [11]. In addition, based on these effects, we proposed a walking method for legged rovers that reduces the distance they slip on loose ground. The effectiveness of the proposed walking method was evaluated by conducting an experiment in which a legged testbed walked on loose ground. The experimental results showed that the walking distance realized based on the proposed walking method was longer than that without vibration.

In the proposed walking method, the bearing capacity is increased by vibrating the loose soil on the ground. The running performance of a legged rover is considered to be related to the bearing capacity, which is the resistance force exerted on the legs of the rovers by the ground. Understanding the relationship between the bearing capacity and vibration parameters is essential to clarify the mechanism whereby the bearing capacity is increased by imparting vibrations. This relationship offers valuable information as a design guideline for the walking motion because a suitable vibration can be selected to prevent the rover from slipping.

Compaction of the ground by vibration is also used in the civil engineering field to construct the foundation of buildings. The relationship between the machine that compacts the ground and the conditions of the ground has been investigated. Hashimoto et al. studied the compaction performance of small-vibration compactors and proposed an evaluation method for this performance [12]. Gao et al. investigated a specific ground condition compacted using a vibratory probe and considered this mechanism [13]. The vibratory probe can effectively compact the ground because it vibrates within the ground. In the construction of foundations, the work involving the compaction of the ground and the evaluation of the compaction effect are generally separate [14]. The reason is that it is possible to make enough time to evaluate the compaction effect after imparting vibration. Therefore, these studies focused on an evaluation method for compacted ground. A method to rapidly assess the condition of the ground is necessary when the compaction effect of vibration is to be used to walk the rover. Moreover, the energy efficiency of the rover is important for planetary exploration. A detailed investigation of the relationship between the change in the compactness of the ground

and the vibration parameters would instantly provide information about the condition of the ground and promote energy saving.

Figure 1 shows an overview of this study. A previous study led to the proposal of a walking method that relied on the use of vibrations to prevent legged rovers from slipping on loose ground (Fig. 1a). The running performance was improved by employing the proposed walking method. Increasing the bearing capacity by imparting vibrations is significant for preventing slipping. Therefore, the relationship between the bearing capacity and vibration parameters must be clarified to enhance the usefulness of this phenomenon. In this study, we attempted to clarify this relationship by following two approaches (Fig. 1b) and studied the frequency, amplitude, and vibration acceleration as vibration parameters.

1 Investigation of the relationship between the bearing capacity and vibration parameters (frequency, amplitude, and vibration acceleration)
2 Comparison between frequency and amplitude as vibration parameters in relation to increasing the bearing capacity

To improve the proposed walking method, we plan to propose a model that estimates the increase in the bearing capacity as a result of vibration in a future study based on the results of this study (Fig. 1c).

The remainder of this paper explains the mechanisms that govern the slippage of legged rovers on loose ground. The proposed walking method with vibration is described in the "Study background" section. Second, the relationship between the bearing capacity and vibration parameters is investigated. In this study, the increase in the bearing capacity by imparting vibrations

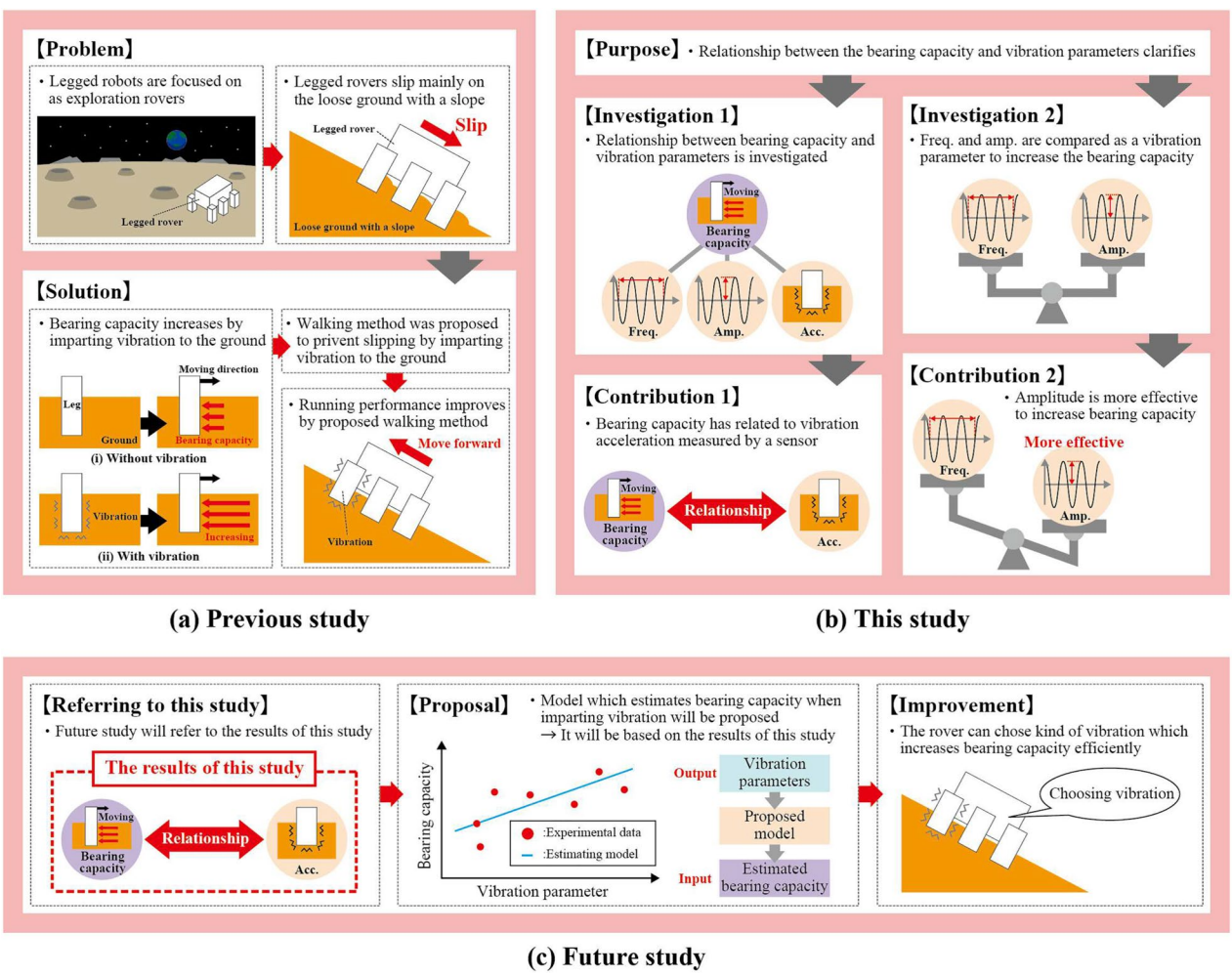

Fig. 1 Evolution of the current study

was measured under different experimental conditions related to the vibration frequency and amplitude. In the experiment, a rod was lowered to the ground and vibrated. The bearing capacity was measured when the rod was dragged on the ground. Third, the relationship between the bearing capacity and the actual vibration acceleration was investigated. This acceleration was measured by attaching an acceleration sensor to the rod. Fourth, the frequency and amplitude were compared as vibration parameters that could be used to increase the bearing capacity, which was measured using high-frequency and high-amplitude vibrations with the same accelerations. Moreover, the actual vibration acceleration was measured when the rod was lowered to the ground. In this experiment, the changes in vibrations inside the ground were investigated. Finally, the "Conclusions" section summarizes this study.

The contributions of this study are as follows. The bearing capacity is related to the actual vibration acceleration measured by an acceleration sensor. This experimental result suggests that the bearing capacity can be estimated from vibration acceleration. Moreover, the amplitude is more effective in increasing the bearing capacity than the frequency because high-amplitude vibrations generate larger additional vibrations by the collision between the rod and the ground than high-frequency vibrations. This knowledge is valuable for selecting a suitable vibration that can efficiently increase the bearing capacity.

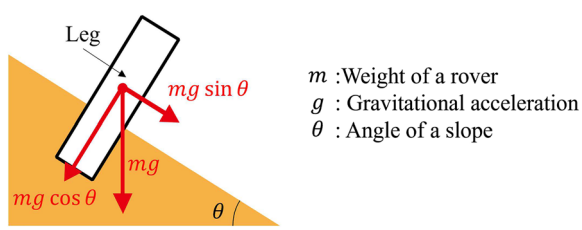

Fig. 2 Force exerted by a leg on sloped ground

Study background

Slippage mechanisms of legged rovers on sloped loose ground

Figure 2 shows the force that a leg of the rover applies to sloped ground. The leg of the rover exerts shear force on the ground in the downslope direction. As the angle of the slope increases, the shear force applied to the ground also increases. We confirmed that when the rod is dragged on the ground, the bearing capacity the leg receives from the ground changes, as shown in Fig. 3 [15]. The ground crumbled when the bearing capacity reached its maximum value (Fig. 3b). Based on the change in the bearing capacity, we consider that legged rovers slip when the shear force exceeds the maximum value of the bearing capacity (Fig. 4). Therefore, the bearing capacity must be increased to prevent legged rovers from slipping on loose ground.

Previously proposed walking method using vibration to prevent a legged rover from slipping

Previously, we proposed a walking method based on vibration to prevent legged rovers from slipping on loose ground [11]. In this section, the changes in the ground when imparting vibrations, and the proposed walking method that uses vibrations are explained.

First, the changes in the ground when imparting vibrations are explained. Figure 5 shows the movement of the ground particles when vibrations are imparted to the ground. Spaces existed between the particles before vibrations were imparted (Fig. 5a). These particles moved when vibrations were imparted to the ground, as shown in Fig. 5b. The shear strength of the ground decreased because the contacts of particles were released. Moreover, the vibrator easily sinks into the ground by

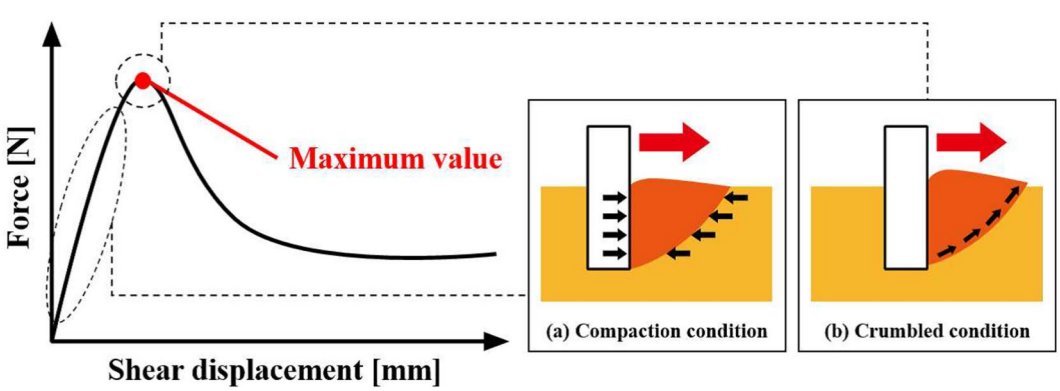

Fig. 3 Bearing capacity versus shear displacement

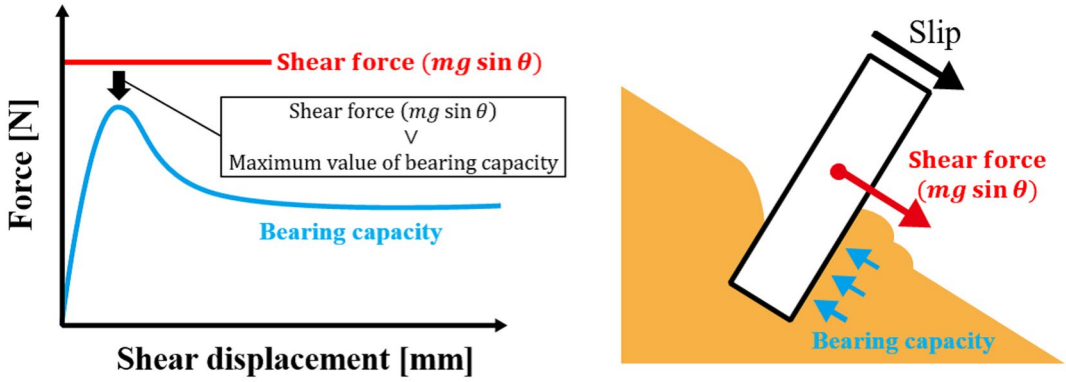

(a) Condition that a shear force is larger than the bearing capacity **(b)** Condition that a leg of a rover slips

Fig. 4 Overview of leg slippage

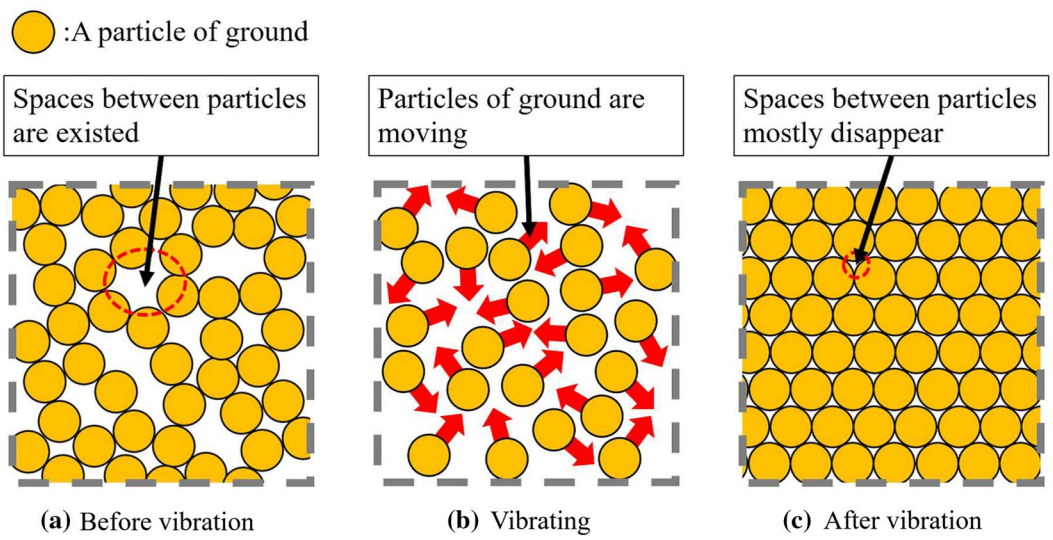

(a) Before vibration **(b)** Vibrating **(c)** After vibration

Fig. 5 Movement of particles comprising the ground when vibrations are imparted

decreasing the shear strength [16]. After the vibration ceased, the ground was compacted because the spaces between the particles had mostly disappeared (Fig. 5c). Under these ground conditions, the shear strength and density increase [17].

Next, we describe the proposed walking method. This method increases the sinkage of the legs and density of the ground by imparting vibrations to it. The bearing capacity of the legs also increased owing to an increase in these parameters. Figure 6 shows the movement of the leg and timing of the vibrations of the leg. First, the leg is raised and moved forward (Fig. 6b). Second, the leg moves toward the ground and vibrates (Fig. 6c). This motion increases the sinkage of the leg to the ground because the shear strength of the ground decreases as a result of the vibrations being imparted. Finally, the vibration ceases when the leg ceases to sink into the ground (Fig. 6d). This motion increases the density of the ground, because the ground is compacted after vibrations were imparted. The slip line increases by increasing the sinkage of the legs and density of the ground [18, 19]. The slip line is the border of the area along which the particles move when the leg moves to the ground. The longer the slip line, the larger the bearing capacity becomes (Fig. 7). In our previous study, a legged testbed walked on sloped loose ground to evaluate the effectiveness of the proposed walking method. The experimental results showed that the proposed walking method improved the running performance of a legged rover.

Increasing the bearing capacity by imparting vibrations is significant for the proposed walking method to increase the running performance. Therefore, the relationship between the bearing capacity and vibration parameters must be clarified to

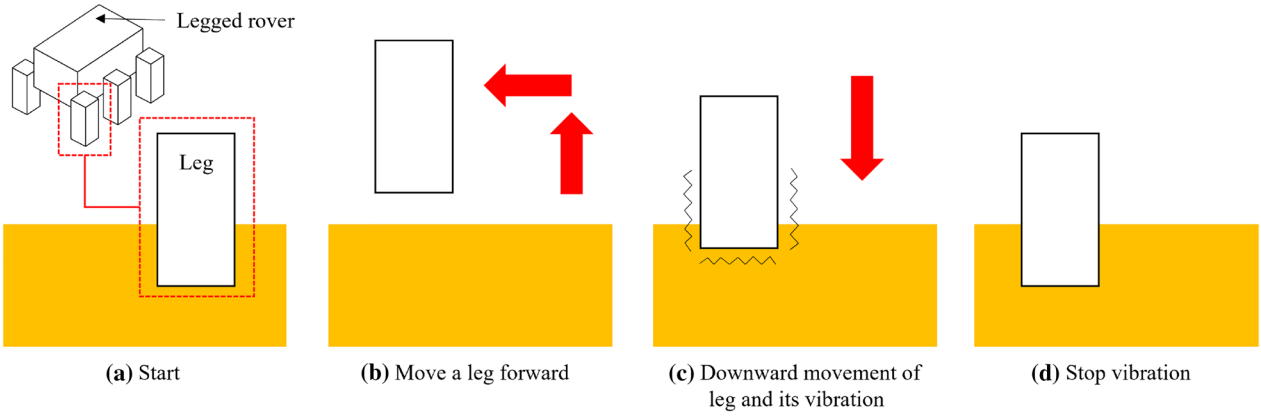

Fig. 6 Vibration timing of the walking method with vibrations proposed in previous study

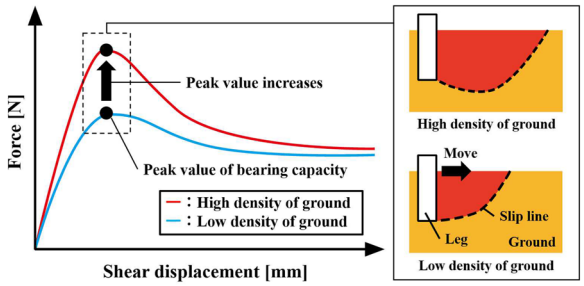

Fig. 7 Relationship between the peak value of the bearing capacity and slip line of the ground

improve the proposed walking method with vibrations. This relationship offers valuable insight into the selection of a suitable vibration to prevent rovers from slipping.

Investigation of the relationship between the bearing capacity and vibration parameters (Vibration frequency and amplitude)

We consider the bearing capacity to be the force that supports the legged rover against gravity in the direction of the slope (Fig. 8a). Investigations of the surfaces of the Moon and Mars show that these contain slopes of approximately 30° as steep slopes [20, 21]. This study focused on the bearing capacity in the horizontal direction. In this experiment, the bearing capacity was measured by dragging a rod horizontally on the ground under different experimental conditions (Fig. 8 (b)).

In the models of bearing capacity, this value is decided from the size of the slip line underground. Because a previous study investigated that the slip line becomes large by vibration [15], we considered that the bearing capacity increases by vibration on the sloped ground. However, there was the possibility that the bearing capacity does not increase on the sloped ground even if

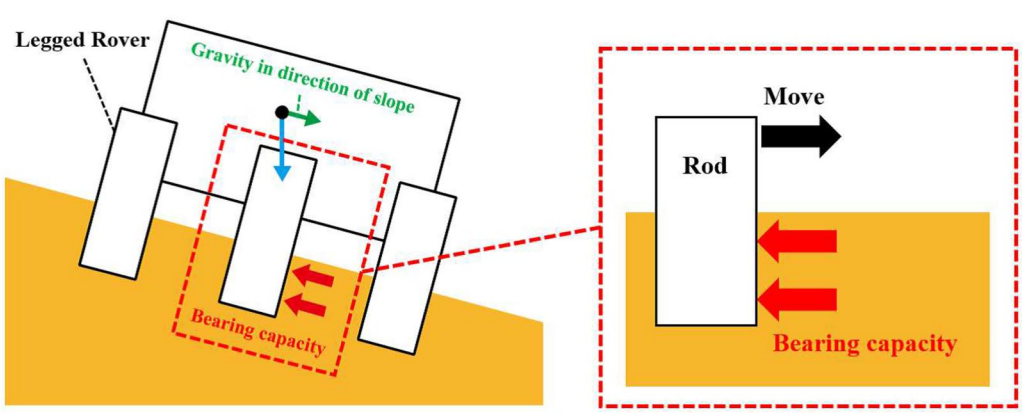

(a) Legged rover on the ground with a slope (b) Environment for measuring bearing capacity

Fig. 8 Actual environment where the legged rover walks and experimental environment for measuring the bearing capacity in the horizontal direction

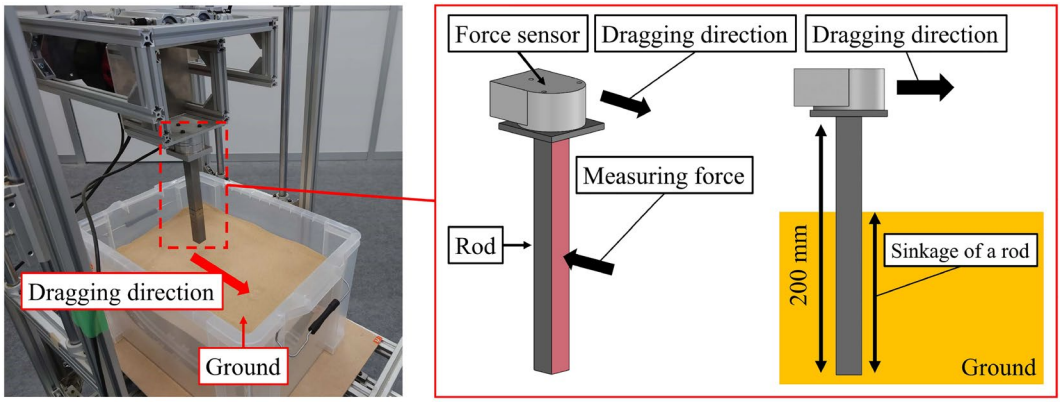

(a) Experimental setup **(b)** Leg part

Fig. 9 Experimental setup for measuring the bearing capacity

vibration imparts to the ground because the gravity of the downslope direction arises and the movement of sand particles changes. Therefore, the bearing capacity on the sloped ground was measured. The details of the method and results are explained in the "Appendix" section. In the results, the bearing capacities on the sloped ground and flat ground were compared and showed a similar relationship with vibration parameters. Therefore, we consider the changes in the bearing capacity in the horizontal direction owing to vibration to indicate a similar tendency under the sloped conditions.

The bearing capacity in the horizontal direction can be easily adapted to conventional models that estimate the lateral bearing capacity. The force exerted when an object is dragged horizontally on the ground is known as the lateral bearing capacity. In a future study, we plan to construct a model that estimates the bearing capacity in the horizontal direction, which is increased by vibration, based on the results of this study. After constructing the proposed model, it will be improved to include the condition of sloped ground. The experimental conditions that were varied were the vibration frequency and amplitude. We planned this experimental method with reference to related studies that measured the force when an object was dragged horizontally on the ground [22, 23].

Experimental methods

Figure 9 shows the experimental setup that consists of a soil tank, rod, and force sensor. The soil tank had a length, width, and height of 309, 439, and 300 mm, respectively. The ground material consisted of Silica No. 5. This sand is widely used in studies of planetary exploration rovers [24–26]. Table 1 lists the parameters of the sand. Figure 10 shows the size of the rod, which is a quadrangular prism. The bottom end of the rod is square with sides of 20 mm and the rod was 200 mm long. The rod has a simple shape, which helps measure the increase in the bearing capacity caused by vibrations. The size of the rod was based on that in related studies of planetary exploration rovers with legs [11, 17, 22, 27]. The size of the rod was set similar to the size of the legs used previously. A force sensor was attached to the rod, as shown in Fig. 9b. The force sensor measured the force

Table 1 Parameters and specifications of Silica No.5 [28, 29]

Item	Conditions (value)
Size of particle	150–840 μm
Maximum bulk density	1629 kg/m^3
Minimum bulk density	1320 kg/m^3
Soil cohesion	762 N/m^2
Internal friction angle	32.5 °

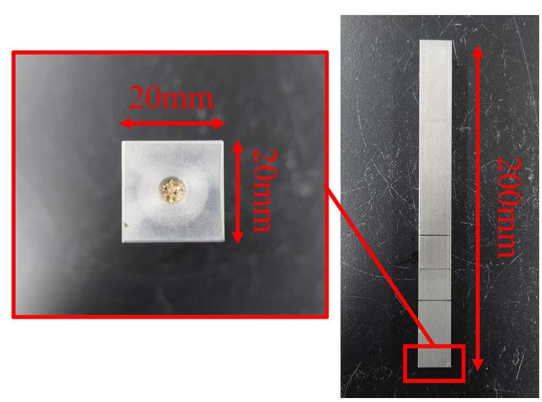

Fig. 10 Overview of a rod

exerted on the red surface of the rod, as shown in Fig. 9b. Figure 9 (b) shows the sinkage of the rod and position of the force sensor. The sinkage of the rod into the ground was set to 30, 50, and 70 mm. This experimental machine was mounted on a vibration generator (Wave Maker 05), which propagates vibrations to the rod. The direction of the vibrations was the same as that of the dragging direction of the rod. The vibration waveform was a sine wave. Figure 11 shows the details of the vibration. The frequency of the vibration was set to 10, 30, and 50 Hz. The amplitude of the vibration was set to 0.4, 0.5, and 0.6 mm. These values represent the total amplitudes.

Figure 12 illustrates the flow of the experiment. First, the ground was mixed and flattened. Then, the rods were placed on the ground. Next, vibration was generated for 200 s. Subsequently, the rod was dragged 13 mm at a speed of 0.13 mm/s. The force sensor registered the bearing capacity value. The bearing capacity without vibrations was also measured. Five trials were performed for each experimental condition. Table 2 presents the experimental conditions.

Experimental results and discussion

The variation in the bearing capacity against the shear displacement exhibited two types of shapes (Fig. 13). The type of variation shown in Fig. 13a was observed in certain experiments without vibration. In this type, the bearing capacity initially increased, where after it converged with the peak value, which was obtained by measuring the converged value of the bearing capacity. The type of variation in Fig. 13 (b) was observed in all experimental results when vibration was imparted and for some experimental results without vibration. In this type, the bearing capacity initially increased, after which

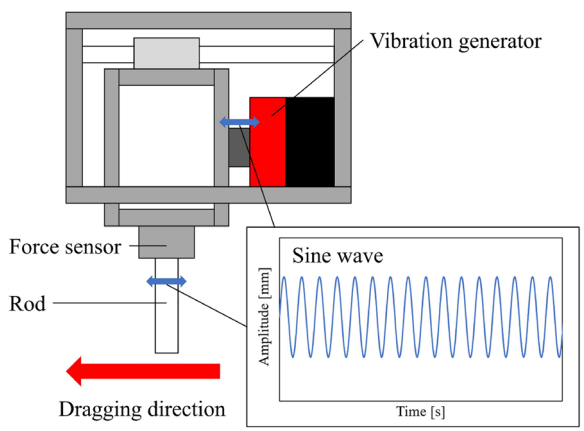

Fig. 11 Mechanism of vibration generation

Table 2 Experimental conditions for measuring the bearing capacity

Item	Conditions (value)
Number of trials	5
Sinkage of rod	30 mm, 50 mm, 70 mm
Vibration time	200 s
Traction speed	0.13 mm/s
Traction distance	13 mm
Type of sand	Silica No.5
Vibration generator	Wave Maker 05
Vibration frequency	10 Hz, 30 Hz, 50 Hz
Vibration amplitude	0.4 mm, 0.5 mm, 0.6 mm (Total amplitude)
Force sensor	PFS055YA251U6

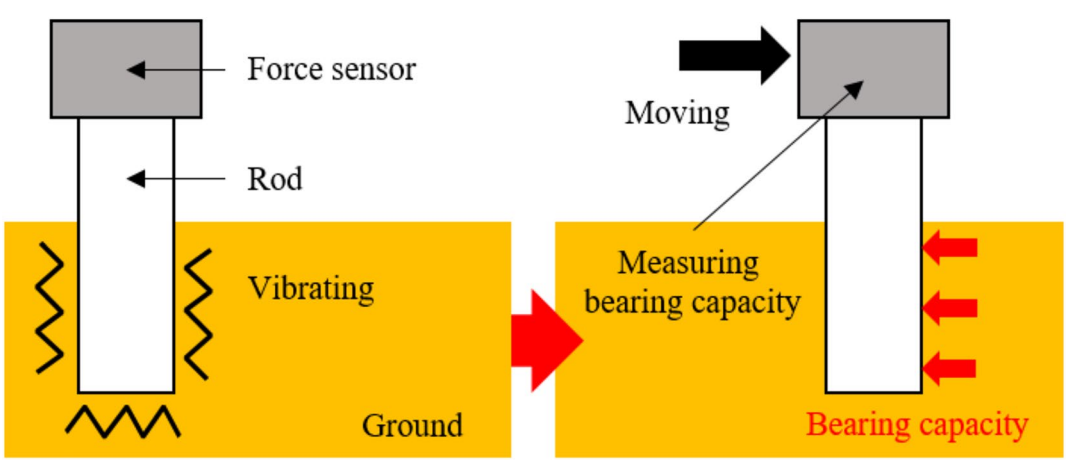

Fig. 12 Experimental flow for measuring the bearing capacity

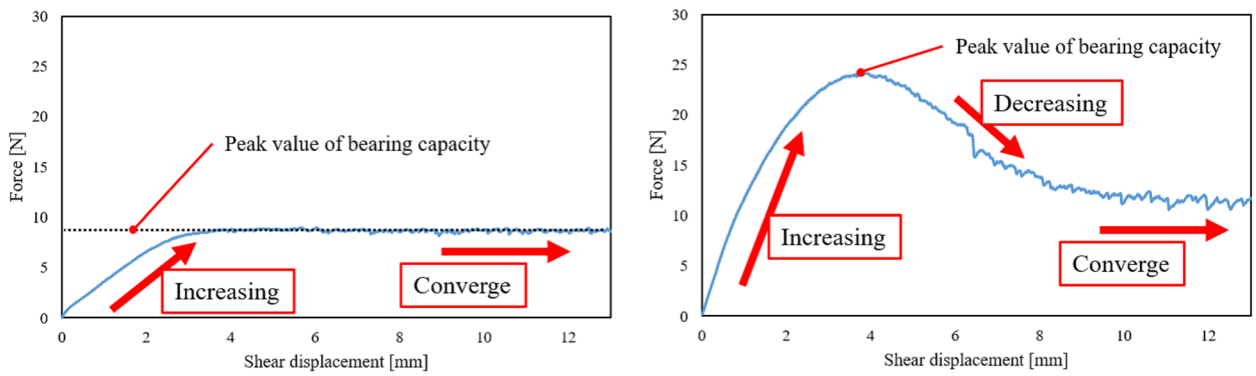

(a) Rod sinkage: 50 mm, No vibration

(b) Rod sinkage: 50 mm, Vibration freq.: 50 Hz, Amp.: 0.5 mm

Fig. 13 Bearing capacity versus shear displacement

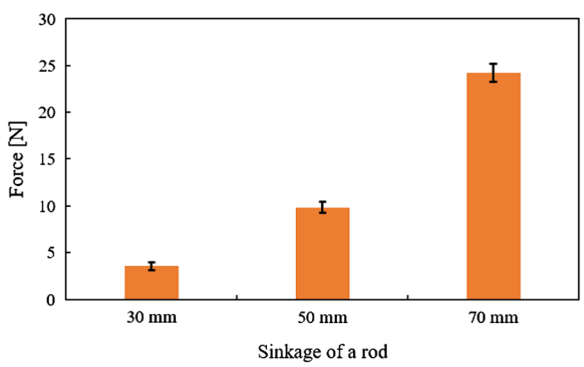

Fig. 14 Comparison of the bearing capacity without vibration

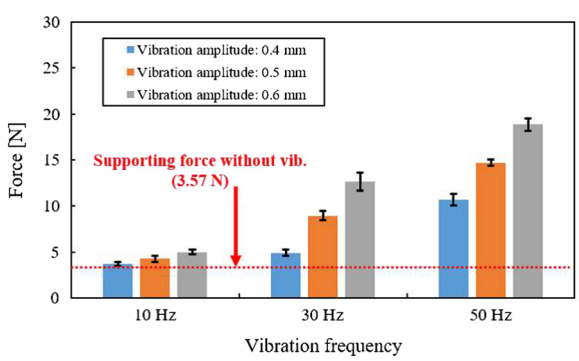

Fig. 15 Comparison of the bearing capacity (Rod sinkage: 30 mm)

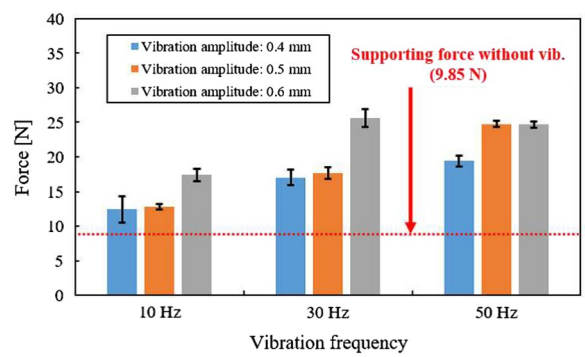

Fig. 16 Comparison of the bearing capacity (Rod sinkage: 50 mm)

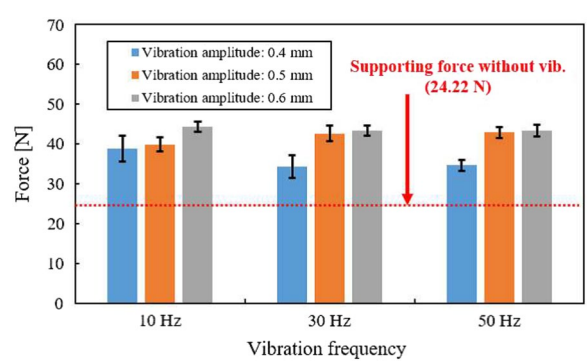

Fig. 17 Comparison of the bearing capacity (Rod sinkage: 70 mm)

it decreased and converged. The peak value was obtained by measuring the maximum bearing capacity.

Figure 14 shows the peak value of the bearing capacity without vibration as an average of five trials. Figures 15 to 17 show the peak value of the bearing capacity with vibrations as the average of five trials for each sinkage of the rod. These graphs show the standard errors calculated from the five experimental trials. The red line in Figs. 15 to 17 shows the average value of the bearing capacity without vibrations. The bearing capacity with vibrations was larger than that without vibrations under all experimental conditions.

The larger the frequency and amplitude, the larger the bearing capacity when the sinkage of the rod is 30 mm (Fig. 15).

The bearing capacity was not related to the frequency or amplitude when the sinkage of the rod was 50 mm (Fig. 16). When the vibration frequency was 10 and 30 Hz, the bearing capacity obtained by setting the amplitude of vibration to 0.4 mm was approximately the same as that obtained for an amplitude of vibration of 0.5 mm. When the vibration frequency was 50 Hz, the bearing capacity obtained using an amplitude of vibration of 0.5 mm was approximately the same as that obtained for an amplitude of vibration of 0.6 mm.

When the sinkage of the rod was 70 mm, the bearing capacity was not related to the frequency or amplitude because the values of the bearing capacity for each vibration were almost the same (Fig. 17).

These results indicated that the increase in the bearing capacity after vibration was imparted depended on the sinkage of the rod. The pressure exerted on the rod by the earth is not high when the sinkage of the rod is 30 mm. Therefore, the relationship between the bearing capacity and vibration parameters was clearly demonstrated. When the sinkage of the rod was 50 and 70 mm, the relationship between the bearing capacity and vibration parameters was not observed because the vibrations were damped owing to the high pressure exerted by the earth. The larger the sinkage of the rod, the larger the earth pressure (Fig. 18) [19]. Figure 18a shows a passive earth pressure as the earth pressure.

Investigation of the relationship between the bearing capacity and vibration acceleration

The experimental results in the previous section suggest that the vibration experiences damping when the sinkage of the rod is large. For these experiments, it was necessary to identify a parameter that has a strong relationship with the bearing capacity under this condition. We consider the vibration acceleration that is actually imparted to the ground to be related to the bearing capacity because it includes the damping effect. In this experiment, the vibration acceleration was measured using an acceleration sensor, and the relationship between the bearing capacity and actual vibration acceleration was investigated.

Experimental methods

The experimental setup is the same as that described in the previous section (Fig. 9). The ground material consisted of Silica No. 5. The sinkage of the rod to the ground was set to 30, 50, and 70 mm.

Figure 19 illustrates the flow of the experiment. First, the ground is mixed and flattened. Then, the rods were placed on the ground. The shape of the rod is illustrated in Fig. 10. Subsequently, vibrations were generated for 200 s, whereupon the vibration acceleration of the rod was measured. Figure 20a shows the mounting position of the cover that stores the acceleration sensor. Figure 20b shows the shape and size of the cover. An acceleration sensor was mounted on top of the cover (Fig. 20b). The acceleration was measured in the x-direction, as shown in Fig. 21. This direction was the same as that of the vibration. The sampling frequency of the vibration acceleration was 400 Hz. Subsequently, the rod was dragged after the vibration ceased. The force sensor registered the bearing capacity value. The relationship between the bearing capacity and actual vibration acceleration was investigated using combinations of these measurements. Five trials were performed for each experimental condition. Table 3 lists the experimental conditions used.

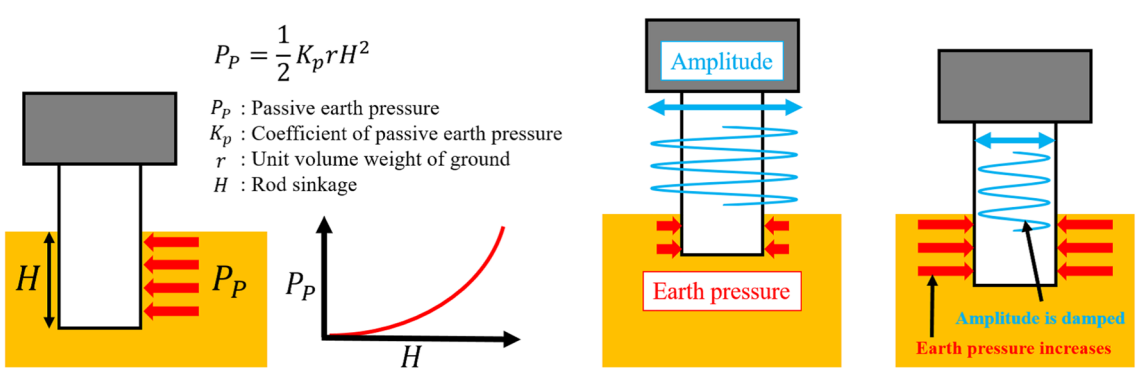

(a) Relationship between passive earth pressure and rod sinkage (b) Low amount of sinkage (c) High amount of sinkage

Fig. 18 Earth pressure corresponding to the sinkage of the rod [19]

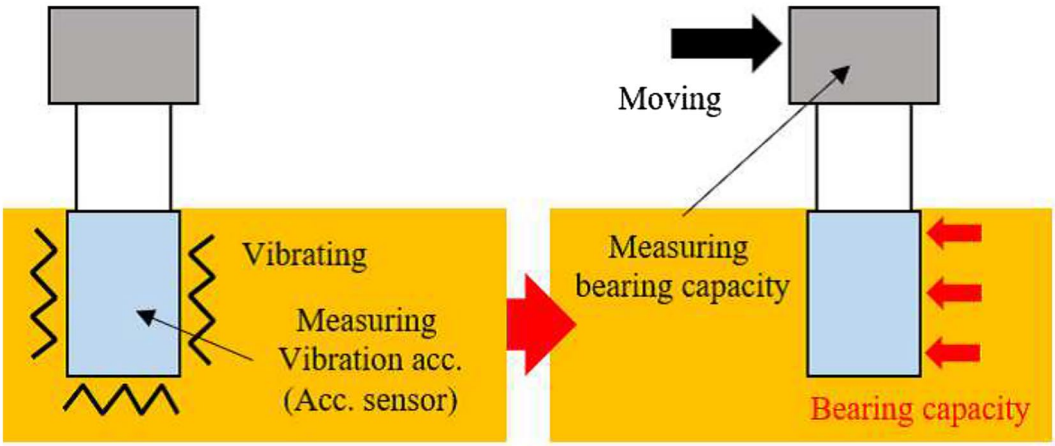

Fig. 19 Experimental flow for measuring the vibration acceleration and the bearing capacity

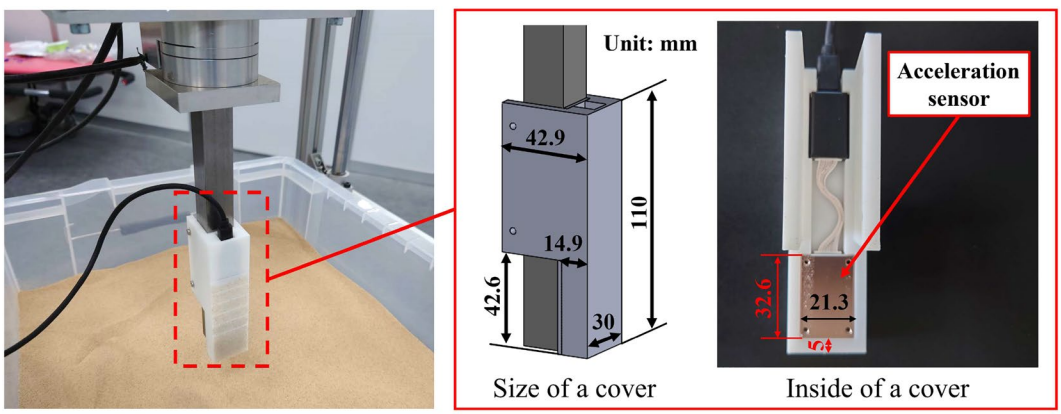

(a) Experimental setup **(b)** Acceleration sensor

Fig. 20 Attachment position of the acceleration sensor

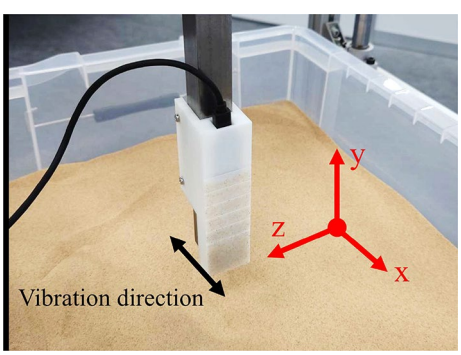

Fig. 21 Direction of measurement of the vibration acceleration

Experimental results and discussion

As an example, Fig. 22a shows the experimental data (sinkage of the rod is 70 mm, frequency is 50 Hz, amplitude is 0.5 mm). In this experiment, the amplitude of the vibration acceleration was initially unstable, but gradually stabilized until it remained constant. In this study, the acceleration amplitude, whose frequency is the same as that of the output, and the root mean square (RMS) were derived from the wave of the vibration acceleration to investigate the relationship with the bearing capacity.

The acceleration amplitude, whose frequency is the same as that of the output, can indicate the damping, which affects the vibration set by the vibration generator. To obtain the acceleration amplitude, the last 100 s in the wave of the vibration acceleration were subjected to fast Fourier transform because the amplitude of the vibration acceleration was constant during the final 100 s (Fig. 22b). The acceleration amplitude, whose frequency is the same as that of the output, was selected from the result of the fast Fourier transform.

The root mean square (RMS) is defined as the square root of the mean square. In some studies, the RMS value

Table 3 Experimental conditions for measuring the vibration acceleration and the bearing capacity

Item	Conditions (value)
Number of trials	5
Sinkage of rod	30 mm, 50 mm, 70 mm
Measuring time of vibration acceleration	200 s
Vibration time	200 s
Traction speed	0.13 mm/s
Traction distance	13 mm
Type of sand	Silica No. 5
Vibration generator	Wave Maker 05
Vibration frequency	10 Hz, 20 Hz, 30 Hz, 40 Hz, 50 Hz
Vibration amplitude	0.5 mm (Total amplitude)
Force sensor	PFS055YA251U6
Acceleration sensor	AccStick6
Sampling frequency of vibration acceleration	400 Hz

was calculated from the acceleration to compare the wave of acceleration [30, 31]. The analyzed results of the wave by the fast Fourier transform include not only the frequency which is the same as the output but also the frequencies which are multiple of the output frequency (Fig. 22b). These frequencies occur by the collision between the rod and the ground [32]. The RMS value can include these frequencies and be used to evaluate the actual vibration wave. The RMS values were calculated using Eq. (1) as follows:

$$a_{rms} = \sqrt{\frac{1}{T}\int_0^T a_{exp}(t)^2 dt} \tag{1}$$

where T is the total vibration time and $a_{exp}(t)$ is the measured vibration acceleration. Figure 23 shows the procedure for calculating the RMS value. The RMS value was calculated from the last 100 s of the measurement data (Figs. 23a and b). First, the DC value is obtained by applying fast Fourier transform to the vibration acceleration wave (Fig. 23c). We define the DC value as the distance between the time axis and center of the vibration acceleration wave. Next, the wave of vibration acceleration was moved to the center of the time axis of the graph based on the DC value (Fig. 23d). Finally, the RMS value is calculated from the edited wave (Fig. 23e).

Figure 24 shows the acceleration amplitude as the average of five trials for each sinkage of the rod. These graphs show the standard errors calculated from the five experimental trials. The acceleration amplitude and RMS values are shown in (a) and (b). The larger the sinkage of the rod, the smaller these values. This result suggests the larger the sinkage of the rod, the more the vibrations were damped. These values using the vibration (Amp. 0.5 mm, Freq. 50 Hz) were extremely higher than others.

Figures 25, 26, 27 and 28 show the vibration acceleration against the bearing capacity. The combinations of the bearing capacity and vibration acceleration are plotted in these figures. The acceleration amplitude and RMS values are shown in (a) and (b). Figures 26 to 28 show the linear approximation and the coefficient of determination.

When the sinkage of the rod was 30 mm, there were two groups of plots with low and high vibration acceleration (Fig. 25). Plots with high vibration acceleration were obtained when the vibration (Amp. 0.5 mm, Freq. 50 Hz) was used. The reason for the high vibration acceleration measured when using the vibration (Amp. 0.5 mm, Freq. 50 Hz) is that the movement of ground particles is different from that using other vibrations. Baumgartner et al. investigated the movement of ground particles when imparting vibration to understand the movement of the sandfish skink, which is a lizard with the ability

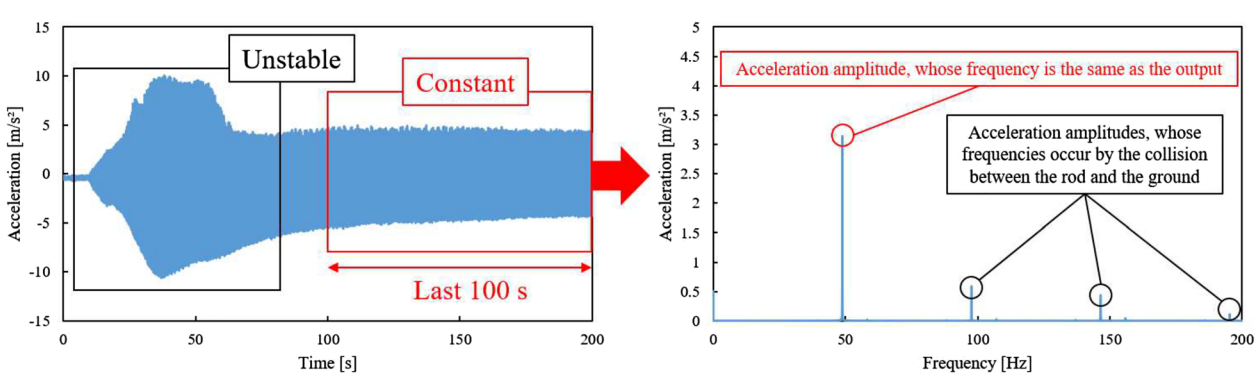

(a) Experimental data (b) Perform FFT to experimental data

Fig. 22 Procedure for obtaining the acceleration amplitude (Using experimental data - Rod sinkage: 70 mm, Vibration frequency: 50 Hz, Amplitude: 0.5 mm)

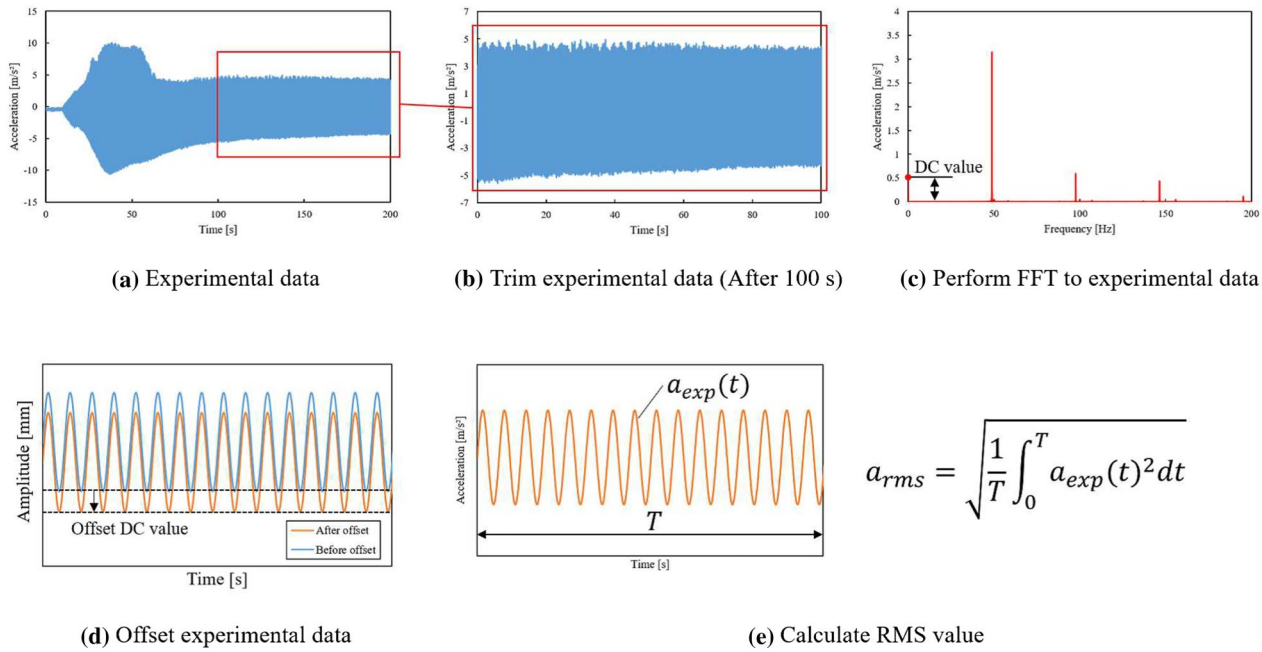

(a) Experimental data **(b)** Trim experimental data (After 100 s) **(c)** Perform FFT to experimental data

(d) Offset experimental data **(e)** Calculate RMS value

Fig. 23 Procedure for calculating the RMS value (Using experimental data - Rod sinkage: 70 mm, Vibration frequency: 50 Hz, Amplitude: 0.5 mm)

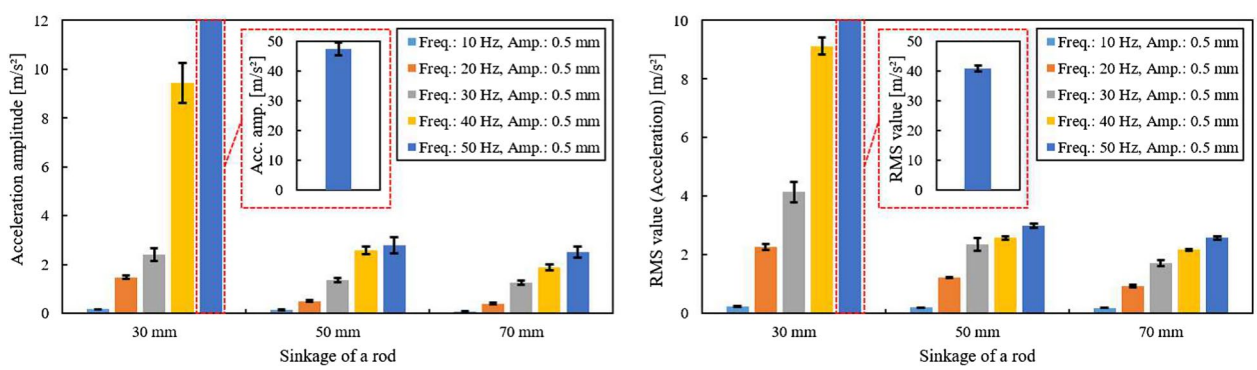

(a) Acceleration amplitude **(b)** RMS value

Fig. 24 Comparison of vibration acceleration

to move through desert sand [33]. They discovered that vibration renders a local decompaction of the sand surrounding the vibrator, suggesting that high-frequency vibration causes the sand to behave like a fluid. Moreover, they confirmed that the earth pressure was decreased by imparting high-frequency vibrations. Figure 29 shows the relationship between the movement of particles and vibration frequency. At low vibration frequencies, the particles remain in contact and move with the rod. In this condition, the ground is compacted. At high vibration frequencies, the particles separate because of collisions. In this condition, the ground behaves like a fluid. From a related study, we consider the behavior of the ground particles when using the vibration (Amp. 0.5 mm, Freq. 50 Hz) to resemble that of a fluid, and the earth pressure to decrease. Therefore, the vibration acceleration was possibly hardly damped by the earth pressure.

The plots obtained using the vibration (Amp. 0.5 mm, Freq. 50 Hz) were excluded in Fig. 26 because the movement of ground particles was possibly different from that in other experimental conditions. Figure 26 shows that the coefficient of determination for the acceleration amplitude was 0.7351, and that of the RMS value was 0.8474. The coefficient of determination in the RMS value was over 0.75 when the sinkage of the rod was 50 and 70 mm. The coefficient of determination of

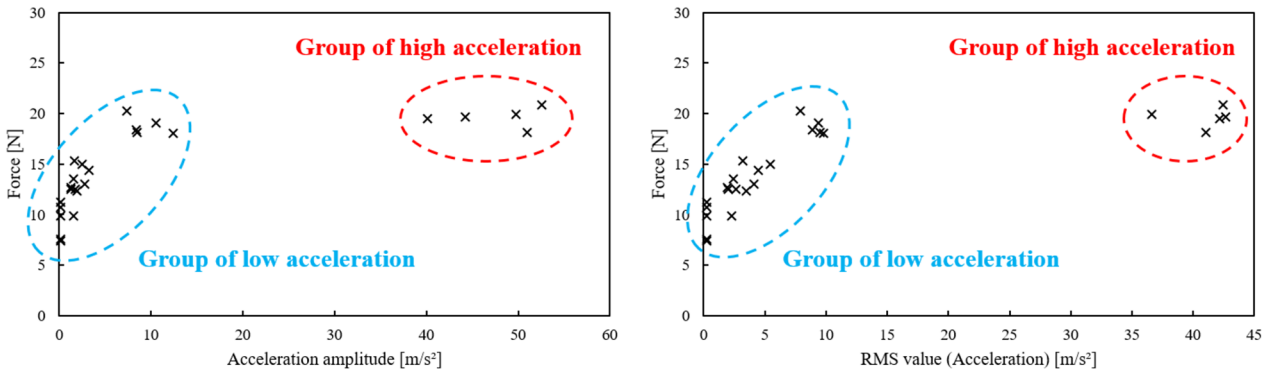

(a) Acceleration amplitude versus bearing capacity **(b)** RMS value versus bearing capacity

Fig. 25 Vibration acceleration versus bearing capacity (Rod sinkage: 30 mm)

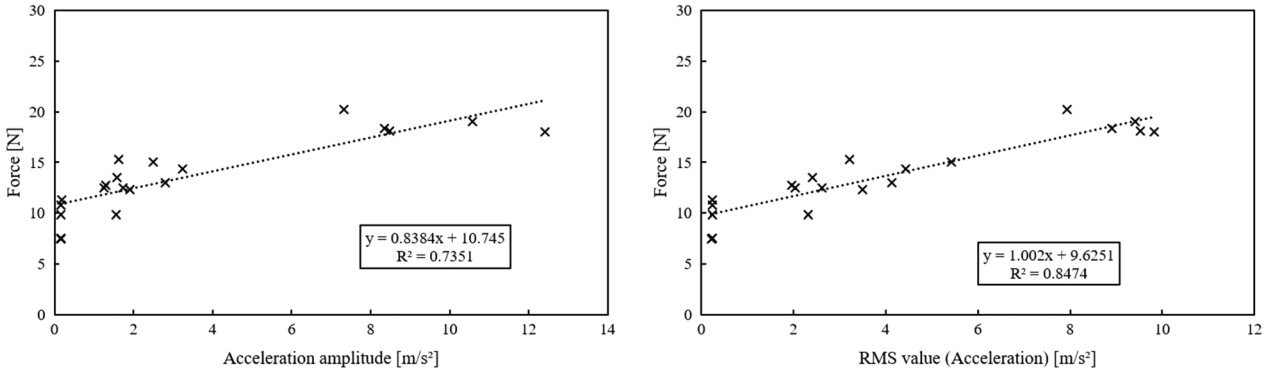

(a) Acceleration amplitude versus bearing capacity **(b)** RMS value versus bearing capacity

Fig. 26 Vibration acceleration versus bearing capacity (Rod sinkage: 30 mm, except data when the vibration (Amp. 0.5 mm, Freq. 50 Hz) was used)

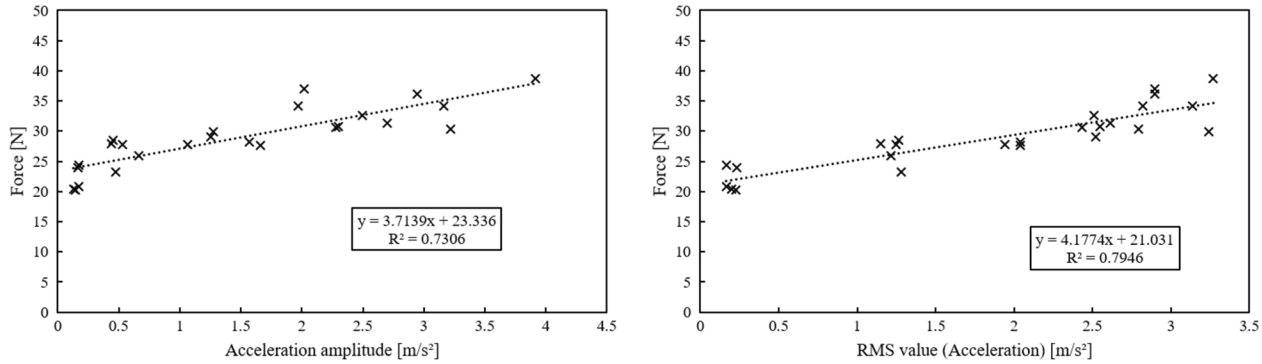

(a) Acceleration amplitude versus bearing capacity **(b)** RMS value versus bearing capacity

Fig. 27 Vibration acceleration versus bearing capacity (Rod sinkage: 50 mm)

the acceleration amplitude was smaller than the RMS value when the sinkage of the rod was 50 and 70 mm. Therefore, the RMS value was correlated with the bearing capacity. We consider that the vibrations which occur by the collision between the rod and the ground also work to increase the bearing capacity. This experimental result

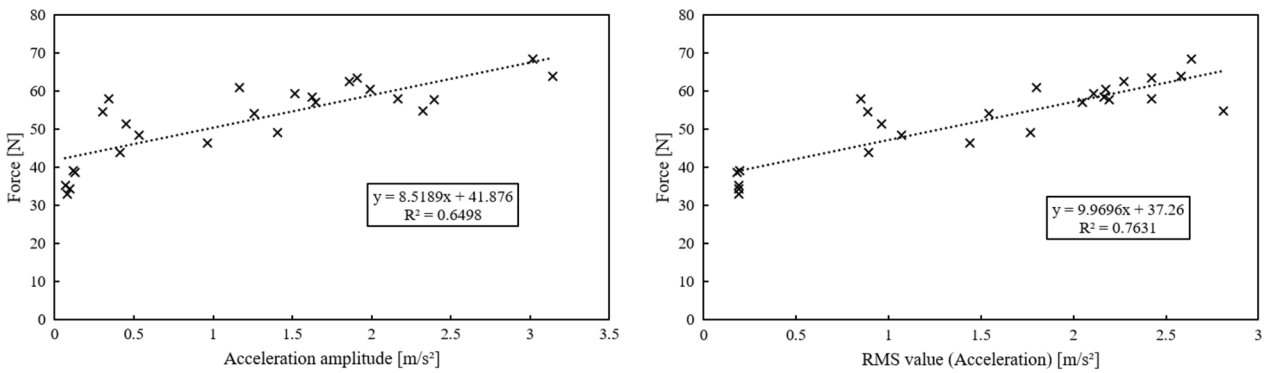

(a) Acceleration amplitude versus bearing capacity

(b) RMS value versus bearing capacity

Fig. 28 Vibration acceleration versus bearing capacity (Rod sinkage: 70 mm)

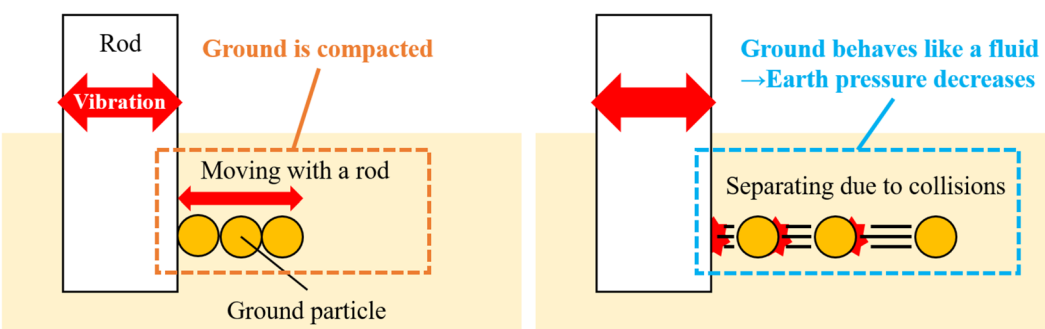

(a) Case of imparting low frequency vibration

(b) Case of imparting high frequency vibration

Fig. 29 Changing movement of particles comprising the ground by kind of vibration

suggests that the bearing capacity can be estimated from the vibration acceleration.

Comparison of the frequency and amplitude as vibration parameters in regards to increasing the bearing capacity

Experimental methods

This investigation compared the frequency and amplitude as vibration parameters with respect to efficiently increasing the bearing capacity. The bearing capacity was measured using vibrations with high frequency and amplitude. Moreover, the vibration acceleration was measured using an acceleration sensor when the rod was on the ground. Table 4 lists the three sets of vibrations. The accelerations of these vibrations were identical. Therefore, a vibration parameter that efficiently increases the bearing capacity can be determined by comparing the bearing capacities obtained for each vibration. These sets changed the acceleration in three steps. The vibration acceleration was calculated using Eq. (2).

Table 4 Combination of vibrations

	Frequency is larger	Amplitude is larger
Set 1	Freq.: 10 Hz	Freq.: 5.8 Hz
(Acc.: 0.99 m/s^2)	Amp.: 0.5 mm	Amp.: 1.5 mm
Set 2	Freq.: 30 Hz	Freq.: 17.3 Hz
(Acc.: 8.88 m/s^2)	Amp.: 0.5 mm	Amp.: 1.5 mm
Set 3	Freq.: 50 Hz	Freq.: 28.9 Hz
(Acc.: 24.67 m/s^2)	Amp.: 0.5 mm	Amp.: 1.5 mm

$$A = \frac{1}{2}D(2\pi f)^2 \tag{2}$$

where A, D, and f represent the vibration acceleration, total amplitude, and frequency, respectively. The experimental method is the same as that described in the previous section (Fig. 19). The bearing capacity and vibration acceleration were measured in this experiment. Table 5 lists the experimental conditions used.

Table 5 Experimental conditions for the comparison of vibration parameters

Item	Conditions (value)
Number of trials	5
Sinkage of rod	30 mm, 50 mm, 70 mm
Vibration time	200 s
Traction speed	0.13 mm/s
Traction distance	13 mm
Type of sand	Silica No.5
Vibration generator	Wave Maker 05
Force sensor	PFS055YA251U6

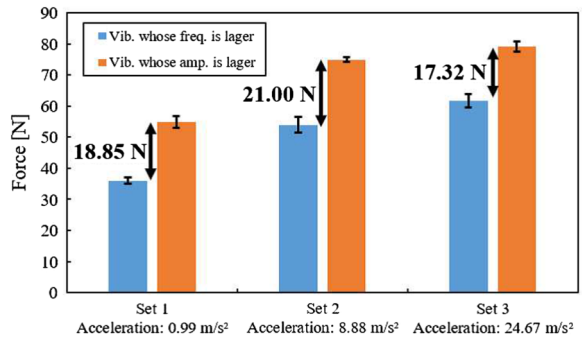

Fig. 32 Bearing capacity in each combination of vibrations (Rod sinkage: 70 mm)

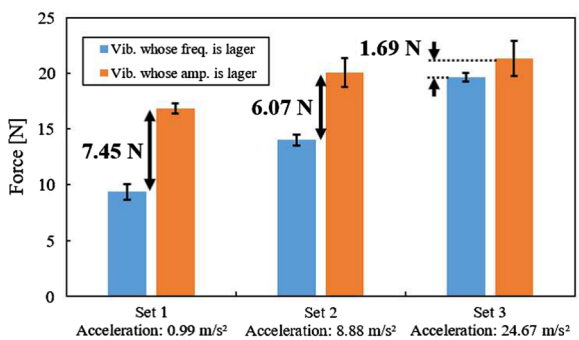

Fig. 30 Bearing capacity in each combination of vibrations (Rod sinkage: 30 mm)

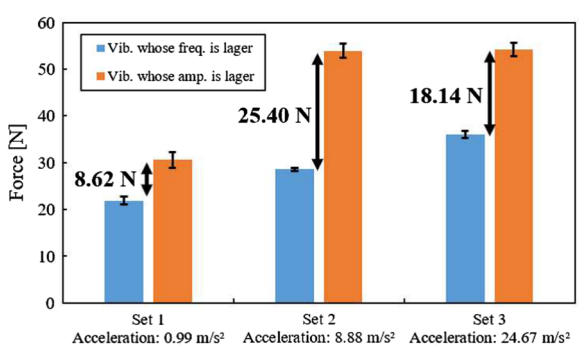

Fig. 31 Bearing capacity in each combination of vibrations (Rod sinkage: 50 mm)

Experimental results and discussion

Figures 30, 31, 32 show the peak value of the bearing capacity with vibration. These results are the averages of five trials for each sinkage of the rod. These graphs show the standard errors calculated from the five experimental trials.

For each sinkage of the rod, the bearing capacity obtained using the high-amplitude vibration was larger than that obtained using the high-frequency vibration in each set of vibration combinations (Figs. 30,31, 32). These experimental results indicate that the amplitude is more effective for increasing the bearing capacity than the frequency.

Figures 33, 34, 35 show the acceleration amplitude and the RMS value for each sinkage of the rod. The acceleration amplitude and RMS values are shown in (a) and (b), respectively. These graphs show the standard errors calculated from the five experimental trials.

When the sinkage of the rod was 30 mm, the acceleration amplitude and RMS value obtained for the high-amplitude vibration were larger than those obtained for the high-frequency vibration in sets 1 and 2 of the vibration combinations (Fig. 33). When the sinkage of the rod was 30 mm, the bearing capacity obtained using the high-amplitude vibration was larger than that obtained using the high-frequency vibration in sets 1 and 2 of the vibration combinations (Fig. 30). These experimental results show that a relationship exists between the actual vibration acceleration and bearing capacity. The acceleration amplitude and RMS value obtained for the high-frequency vibration were larger than those obtained for the high-amplitude vibration in set 3 (Fig. 33). As mentioned in the previous section, we attributed the high vibration acceleration that was measured when using the vibration conditions (Amp. 0.5 mm, Freq. 50 Hz) to the behavior of the ground particles, which resembled that of a fluid, and the decrease in the earth pressure. Therefore, the vibration acceleration was possibly hardly damped by the earth pressure. It is necessary to distinguish between the results obtained using the vibration conditions (Amp. 0.5 mm, Freq. 50 Hz) and others, because the movement of ground particles could possibly be different from that using other vibrations.

When the sinkage of the rod was 50 mm, the acceleration amplitude obtained for the high-amplitude vibration was larger than that obtained for the high-frequency vibration in sets 2 and 3 of the vibration combinations

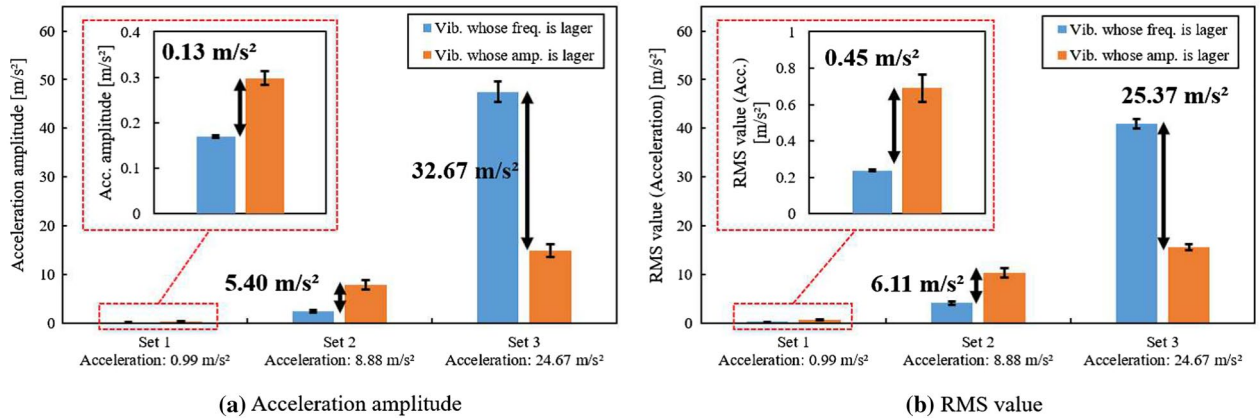

(a) Acceleration amplitude (b) RMS value

Fig. 33 Vibration acceleration in each combination of vibrations (Rod sinkage: 30 mm)

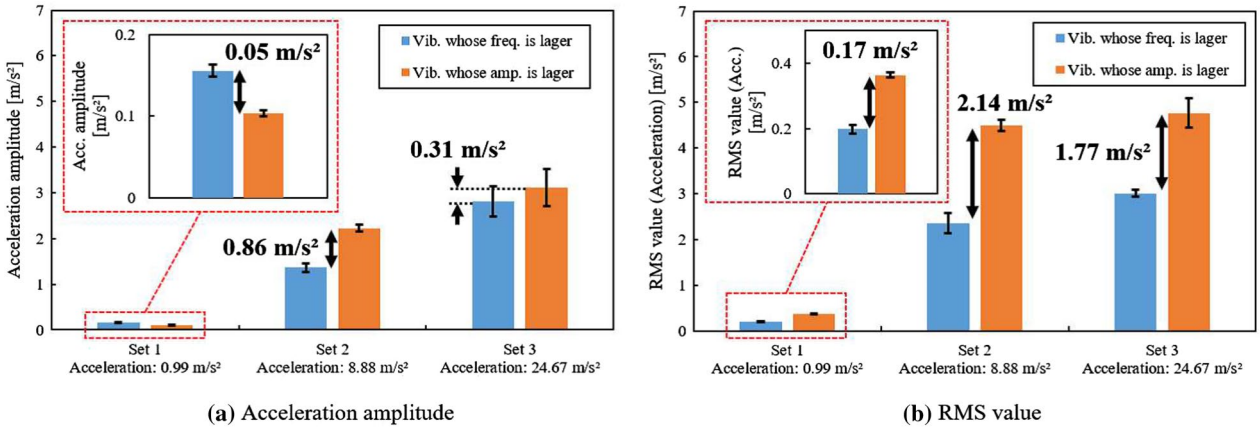

(a) Acceleration amplitude (b) RMS value

Fig. 34 Vibration acceleration in each combination of vibrations (Rod sinkage: 50 mm)

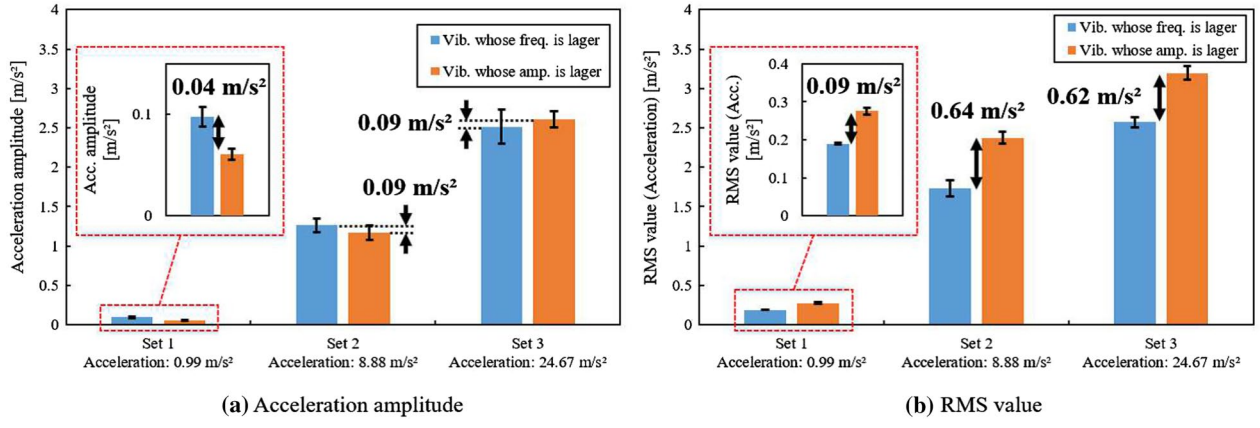

(a) Acceleration amplitude (b) RMS value

Fig. 35 Vibration acceleration in each combination of vibrations (Rod sinkage: 70 mm)

(Fig. 34a). The RMS value obtained for the high-amplitude vibration was larger than that obtained for the high-frequency vibration for all sets of vibration combinations (Fig. 34b). These RMS values correspond to one of the bearing capacities (Fig. 31).

When the sinkage of the rod was 70 mm, the acceleration amplitude obtained for high-frequency vibration was larger than that obtained for high-amplitude vibration in sets 1 and 2 of the vibration combinations (Fig. 35a). The RMS value obtained for the high-amplitude vibration was larger than that obtained for the high-frequency vibration for all sets of vibration combinations (Fig. 35b). These RMS values match one of the bearing capacities (Fig. 32).

Overall, the RMS values are more similar to the results of the bearing capacity than to those of the acceleration amplitude. Therefore, the acceleration wave must be evaluated not only in terms of the output frequency, but also in terms of the total wave. Moreover, the RMS value obtained for high-amplitude vibration was larger than that obtained for high-frequency vibration. The difference in the RMS value between two vibrations in each set was larger than one in the vibration amplitude. These results suggest that high-amplitude vibration makes larger vibrations by the collision between the rod and the ground than high-frequency vibration. From Fig. 13b, when the rod first started being dragged, the bearing capacity increases roughly in proportion to the distance of dragging the rod. From this result, we consider that vibrations that occur by the collision between the rod and the ground became large by high-amplitude vibration because the high-amplitude vibration makes the force that the rod pushes the ground large. These experimental results enable us to determine the reason why the amplitude is an influential vibration parameter with respect to increasing the bearing capac ity.

Conclusions

In this study, two investigations were conducted to clarify the relationship between the bearing capacity and vibration parameters. First, we investigated the increase in the bearing capacity with changes in the vibration parameters. Our experimental results demonstrated that the bearing capacity is related to the vibration acceleration measured by the acceleration sensor. This experimental result suggests that the bearing capacity can be estimated from the vibration acceleration. Next, the frequency and amplitude were compared as the vibration parameters that increased the bearing capacity. We confirmed that the amplitude was more influential in increasing the bearing capacity than the frequency because the high-amplitude vibration makes large vibrations by the collision between the rod and the ground. This knowledge is valuable for selecting a suitable vibration to efficiently increase the bearing capacity. This study led to the suggestion of a method for facilitating further planetary exploration using legged rovers.

This study showed that the experimental results obtained using certain vibration conditions (Amp. 0.5 mm, Freq. 50 Hz) were significantly different from those obtained using other conditions. The reason is considered that the movement of the ground particles differs from that using other vibrations. Therefore, in future studies, we aim to investigate the movement of ground particles when imparting vibrations.

To confirm the effect of vibration in a more realistic environment, the relationship between the bearing capacity and vibration would have to be investigated using sand, which is a reproduced planetary material, and on sloped ground.

In future studies, we plan to develop a model that estimates the bearing capacity. In the planned model, an acceleration sensor would be attached to the legs of the rover to measure the actual vibration acceleration. The planned model would be designed to estimate the bearing capacity from the actual vibration acceleration because of the relationship between the vibration acceleration and bearing capacity.

Appendix

The experiment was conducted to verify that the bearing capacity in the horizontal direction owing to vibration indicates a similar tendency under the sloped condition. In this experiment, the bearing capacity was measured in the sloped ground.

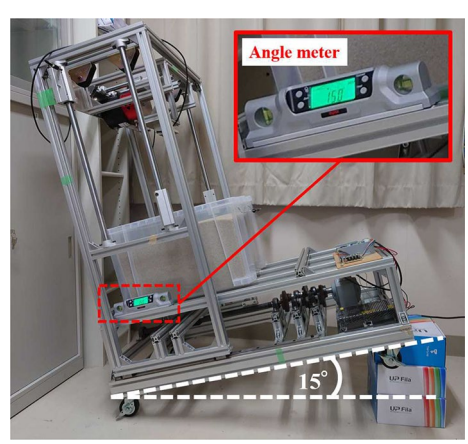

Fig. 36 Tilted experimental setup for measuring the bearing capacity

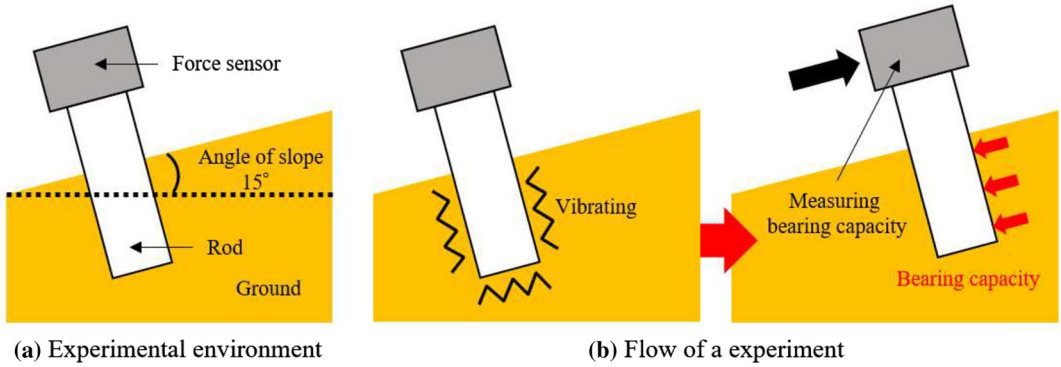

Fig. 37 Environment and flow for measuring the bearing capacity on the sloped ground

Table 6 List of used vibrations for measuring the bearing capacity on the sloped ground

Number	Frequency	Total amplitude
No. 1	10 Hz	0.5 mm
No. 2	30 Hz	0.4 mm
No. 3	30 Hz	0.5 mm
No. 4	30 Hz	0.6 mm
No. 5	50 Hz	0.5 mm

Table 7 Experimental conditions for measuring the bearing capacity on the sloped ground

Item	Conditions (value)
Number of trials	5
Sinkage of rod	50 mm
Vibration time	200 s
Traction speed	0.13 mm/s
Traction distance	13 mm
Type of sand	Silica No.5
Angle of sloped ground	15 degrees
Vibration generator	Wave Maker 05
Force sensor	PFS055YA251U6

Experimental methods

The experimental setup is the same as that described in the previous section (Fig. 9). As shown in Fig. 36, it tilted to 15 degrees to measure the bearing capacity in the sloped ground condition. The ground material consisted of Silica No. 5. The sinkage of the rod to the ground was set to 50 mm.

Figure 37 illustrates the flow of the experiment. First, the ground was mixed and flattened. Then, the rods were placed on the ground. Next, vibration was generated for 200 s. After the vibration ceased, the force sensor set the value to 0 N first and registered the bearing capacity value without the weight of the rod. Subsequently, the rod was dragged 13 mm at a speed of 0.13 mm/s. Five kinds of vibrations were used, as shown in Table 6. The bearing capacity without vibrations was also measured. Five trials were performed for each experimental condition. Table 7 presents the experimental conditions.

Experimental results and discussion

Figure 38a and b show the peak value of the bearing capacity as the average of five trials in the flat and sloped ground conditions. These graphs show the standard errors calculated from the five experimental trials.

In these graphs, the bearing capacity in the sloped ground was smaller than that in the flat ground. The reason is that the weight of the ground in a downslope direction affects the bearing capacity decrease.

Figure 38a compares the bearing capacity in each vibration frequency. Figure 38b compares the bearing capacity in each vibration amplitude. In the sloped ground, the bearing capacity with vibrations was larger than that without vibrations under all experimental conditions. Moreover, the larger the frequency and amplitude, the larger the bearing capacity. These features are almost similar to the results in the flat ground.

From these results, we consider the changes in the bearing capacity in the horizontal direction owing to vibration to indicate a similar tendency in the sloped ground under the experimental condition of this study.

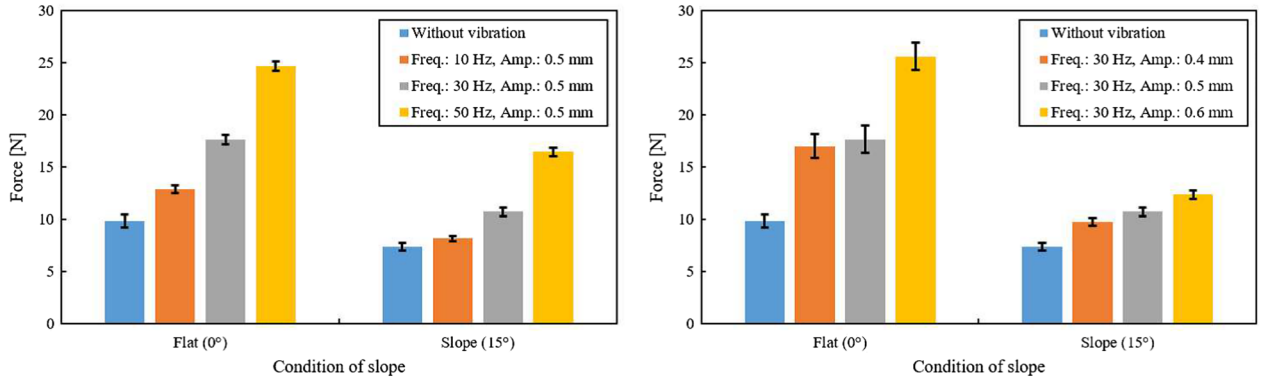

(a) Bearing capacity in each vibration frequency

(b) Bearing capacity in each vibration amplitude

Fig. 38 Comparison of the bearing capacity in each ground condition

Acknowledgements
This study was supported by JSPS KAKENHI (Grant Number JP 21J11944). We would like to thank Editage (www.editage.com) for the English language editing.

Author Contributions
Tomohiro Watanabe wrote the manuscript as the corresponding author. Moreover, he developed the experimental setup and performed experiments. The entire study was supervised by Kojiro Iizuka. All the authors approved the final version of the manuscript.

Funding
The experimental system was funded by JSPS KAKENHI (Grant Number JP 21J11944).

Availability of data and materials
The datasets used in this study are available from the corresponding author upon request.

Declarations

Competing interests
The authors declare that they have no competing interests.

Received: 17 December 2022 Accepted: 10 November 2023
Published online: 27 November 2023

References

1. NASA, Artemis. https://www.nasa.gov/specials/artemis/. Accessed 5 Nov 2023
2. JAXA, International space exploration. https://www.exploration.jaxa.jp/e/program/#slim. Accessed 5 Nov 2023
3. NASA, Gateway. https://www.nasa.gov/gateway. Accessed 5 Nov 2023
4. Fairen AG, Schulze-Makuch D, Rodriguez AP, Fink W, Davila AF, Uceda ER, Furfaro R, Amils R, McKay CP (2009) Evidence for Amazonian acidic liquid water on Mars - A reinterpretation of MER mission results. Pla Spa Sci 57(3):276–287. https://doi.org/10.1016/j.pss.2008.11.008
5. Golombek MP, Cook RA, Economou T, Folkner WM, Haldemann AFC, Kallemeyn PH, Knudsen JM, Manning RM, Moore HJ, Parker TJ, Rieder R, Schofield JT, Smith PH, Vaughan RM (1997) Overview of the mars pathfinder mission and assessment of landing site predictions. Science 278(5344):1743–1748. https://doi.org/10.1126/science.278.5344.1743
6. Witze A (2013) Space rovers in record race. Nature 498:284–285. https://doi.org/10.1038/498284a
7. Kubota T (2001) Mobile explorer robot (Rover) for lunar or planetary exploration. J Jap Soc Mech Eng 104(987):71–74. https://doi.org/10.1299/jsmemag.104.987_71
8. Wilcox BH (2012) ATHLETE:A Limbed Vehicle for Solar System Exploration. In:2012 IEEE Aerospace Conference, IEEE, Big Sky, 3-10 March 2012. https://doi.org/10.1109/AERO.2012.6187269
9. Seidel D, Hermann M, Gumpert T, Loeffl FC, Albu-Schaffer A (2020) Using Elastically Actuated Legged Robots in Rough Terrain: Experiments with DLR Quadruped bert. In:2020 IEEE Aerospace Conference, IEEE, Big Sky, 7-14 March 2020. https://doi.org/10.1109/AERO47225.2020.9172301
10. Colombano S, Kirchner F, Spenneberg D, Hanratty J (2004) Exploration of Planetary Terrains with a Legged Robot as a Scout Adjunct to a Rover. In:Space 2004 Conference and Exhibit, AIAA, San Diego, 28-30 September 2004. https://doi.org/10.2514/6.2004-6095
11. Watanabe T, Iizuka K (2020) Proposal of walking to reduce slipping behavior using compaction effect of loose soil caused by a propagation of vibration for small light lunar planetary exploration rovers with legs. J Jap Soc Mech Eng 86(886):19–00263. https://doi.org/10.1299/transjsme.19-00263
12. Hashimoto T, Fujino K, Tateyama K (2014) Suggestion and application of the peformance index of small compactors in soil compaction. J Jap Soc Civ Eng 70(4):340–352. https://doi.org/10.2208/jscejge.70.340
13. Gao C, Du G, Liu S, He H, Zhang D (2021) The microscopic mechanisms of treating collapsible loess with vibratory probe compaction method. Tra Geo 27:1–15. https://doi.org/10.1016/j.trgeo.2020.100492
14. Nagai H, Kikuchi Y, Noda S, Hyodo T, Tatsuoka F, Kogusuri H, Makabe J (2021) Rationalization of embankment compaction management by fast measurements the soil stiffness index. Geo Soc J 16(1):75–85. https://doi.org/10.3208/jgs.16.75
15. Watanabe T, Iizuka K (2022) Observation of movement of ground particles given vibration when rod is dragged. Int J Eng Tech 14(1):1–8. https://doi.org/10.7763/ijet.2022.v14.1193
16. Watanabe T, Iizuka K (2021) Proposal of walking to prevent a fall of a planetary exploration legged rover using effect of loose soil caused by a propagation of vibration. J Art Int Tech 1(3):153–165. https://doi.org/10.37965/jait.2021.0007
17. Watanabe T, Iizuka K (2020) Study on connection between kind of vibration and influence of ground for leg typed rovers. Int J Mech Eng Robo Res 9(7):979–986. https://doi.org/10.18178/ijmerr.9.7.979-986
18. Wada S, Kouda M, Enami A (1998) Experimental study on passive earth pressure Part 1 The experimental device and an example of the passive earth pressure tests by the device. J Str Con Eng AIJ 63(503):69–76. https://doi.org/10.3130/aijs.63.69_1
19. Terzaghi K, Peck RB (2010) Soil Mechanics in Engineering Practice. Read Books Ltd., United Kingdom
20. Kreslavsky MA, Head JW (2016) The steepest slopes on the Moon from Lunar Orbiter Laser Altimeter (LOLA) Data: Spatial Distribution and

Correlation with Geologic Features. Icarus 273(15):329–336. https://doi.org/10.1016/j.icarus.2016.02.036
21. Aharonson O, Zuber MT, Neumann GA, Head JW III (1998) Mars: Northern hemisphere slopes and slope distributions. Geo Res Let 25(24):4413–4416. https://doi.org/10.1029/1998GL900057
22. Yeomans B, Saaj CM, Winnendael MV (2013) Walking planetary rovers - Experimental analysis and modelling of leg thrust in loose granular soils. J Terramech 50(2):107–120. https://doi.org/10.1016/j.jterra.2013.01.006
23. King RH, Susante PV, Gefreh MA (2011) Analytical models and laboratory measurements of the soil-tool interaction force to push a narrow tool through JSC-1A lunar simulant and Ottawa sand at different cutting depths. J Terramech 48(1):85–95. https://doi.org/10.1016/j.jterra.2010.07.003
24. Mori D, Ishigami G (2015) Excavation model of soil sampling device based on particle image velocimetry. J Terramech 62:19–29. https://doi.org/10.1016/j.jterra.2015.02.001
25. Shirai T, Ishigami G (2015) Development of in-wheel sensor system for accurate measurement of wheel terrain interaction characteristics. J Terramech 62:51–61. https://doi.org/10.1016/j.jterra.2015.09.001
26. Sutoh M (2021) Traveling performance analysis of planetary rovers using a repeatable test system in vacuum. J Terramech 95:15–24. https://doi.org/10.1016/j.jterra.2021.02.003
27. Yeomans B, Saaj CM (2014) Towards terrain interaction prediction for bioinspired planetary exploration rovers. Bioi and Biom 9(1):1–15. https://doi.org/10.1088/1748-3182/9/1/016009
28. Fujiwara D, Tsujikawa N, Oshima T, Iizuka K (2021) Analysis of a resistance force for the locked-wheel of push-pull locomotion rovers using large subsidence. J Terramech 94:1–12. https://doi.org/10.1016/j.jterra.2020.11.004
29. Hara mining Corporation homepage. https://hara-kougyou.co.jp/non-tack/. Accessed 5 Nov 2023
30. Soleimanifar M, Mazaheri M, Schooten KSV, Asgari M, Mosallanezhad Z, Salavati M, Sedaghat-Nejad E, Parnianpour M (2020) Magnitude, symmetry and attenuation of upper body accelerations during walking in women: the role of age, fall history and walking surface. Maturitas 139:49–56. https://doi.org/10.1016/j.maturitas.2020.05.016
31. Spain L, Yang L, Wilkinson JM, McCloskey E (2021) Transmission of whole body vibration - comparison of three vibration platforms in healthy subjects. Bone 144:115802. https://doi.org/10.1016/j.bone.2020.115802
32. Fujiyama T, Tateyama K (2000) The evaluation of compacting ground stiffness by the acceleration of vibratory roller. Jap J JSCE 652:115–123. https://doi.org/10.2208/jscej.2000.652_115
33. Baumgartner W, Fidler F, Weth A, Habbecke M, Jakob P, Butenweg C, Bohme W (2008) Investigating the locomotion of the sandfish in desert sand using NMR-imaging. PLoS ONE 3(10):e3309. https://doi.org/10.1371/journal.pone.0003309

Publisher's Note